ADVANCED OPTICAL MATERIALS
www.advopticalmat.de

Macrocyclic Confined Purely Organic Room-Temperature Phosphorescence Three-Photon Targeted Imaging

*Fang-Fang Shen, Zhixue Liu, Hua-Jiang Yu, Haoran Wang, Xiufang Xu, and Yu Liu**

A purely organic supramolecular assembly emitting three-photon room-temperature phosphorescence (RTP) is constructed from a macrocyclic host, cucurbit[8]uril (CB[8]), and 4-bromophenyl pyridine salt having an alkyl chain length of 6 or 12 carbon atoms (6C and 12C, respectively). Benefiting from macrocyclic host confined guests, the encapsulation of 12C and 6C in the CB[8] cavity results in three-photon absorption and subsequent near-infrared (NIR) phosphorescence emission. Notably, secondary assembly with sulfonated β-cyclodextrin (SCD) further enhances the phosphorescence emission of the multilevel supramolecular assembly. NIR-delayed fluorescence via a light-harvesting phosphorescent energy transfer system is achieved by adding Nile blue as a substrate. Comparison of 12C/CB[8]/SCD and 6C/CB[8]/SCD shows that a long hydrophobic layer is more conducive to stabilizing NIR-delayed fluorescence emission. These findings indicate that multilevel supramolecular assemblies can be used for three-photon-excited NIR-delayed fluorescence and RTP imaging of cancer cells, which greatly expands the biological applications of pure organic RTP materials.

1. Introduction

Room-temperature phosphorescence (RTP) of purely organic supramolecular assemblies is a timely and critical research topic because of its potential significant applications in biology,[1–3] sensing,[4–6] and anti-counterfeiting.[7–10] Its advantages include a long triplet life, large Stokes shift, and easy separation of background signals. However, RTP is easily quenched by dissolved oxygen in aqueous solution, which significantly limits its application in water systems. The key to realizing aqueous RTP emission is to restrict the nonradiative transition of molecules, which involves reducing the vibration and rotation of molecules and shielding oxygen quenchers in water.[11,12] To date, scientists have undertaken considerable endeavors to develop purely organic aqueous RTP materials.[13–15] Among such materials, supramolecular assemblies have emerged as compelling and powerful tools to construct RTP systems through complexation or assembly in water.[16,17] Recently, George and co-workers achieved one of the highest quantum yields for an aqueous RTP system by utilizing a host–guest (cucurbit[7]uril–phthalimide derivative) complex and negatively charged Laponite clay to construct a supramolecular scaffold through electrostatic interactions.[18] Tian et al. and our research group also combined phosphorescent chromophores and supramolecular macrocyclic host molecules to achieve a series of novel and versatile purely organic aqueous RTP emission systems.[19–21]

However, most aqueous RTP systems currently exhibit phosphorescence with a short excitation wavelength, which has lower cell penetrability and greater phototoxicity.[22] Moreover, in addition to small fluorescent organic molecules, the reported near-infrared (NIR) RTP systems mainly contain toxic heavy metals or rare-earth metals, which have potential biological safety issues owing to their long-term retention in the body.[23,24] In recent years, multiphoton imaging materials have drawn much attention owing to their significant advantages of deeper tissue penetration and minimized phototoxicity compared with conventional imaging agents. More recently, Liu and co-workers reported the three-photon fluorescence imaging of lipids using pure organic molecules that exhibit aggregation-induced emission in vivo.[25] In addition, Chao and co-workers reported three-photon phosphorescence bioimaging using cyclometalated Ir(III) complexes.[26] However, pure organic RTP molecules that exhibit a three-photon absorption property have rarely been reported. Therefore, it is necessary to develop purely organic aqueous RTP systems that can undergo simple, convenient, and efficient NIR excitation, especially three-photon excitation.

Here, we report a supramolecular assembly strategy to develop the first purely organic RTP system, exhibiting three-photon absorption and NIR-delayed fluorescence emission for bioimaging (**Scheme 1**). In this study, we designed and synthesized different alkyl-chain-modified bromophenyl pyridinium salts (**6C** and **12C**). The alkyl chain can affect aggregation behavior and is conducive to substrate loading to achieve energy transfer in water.[27,28] As anticipated, bright-green RTP emission was observed upon the formation of a 2:1 supramolecular complex with cucurbit[8]uril (CB[8]). The addition of

F.-F. Shen, Z. Liu, H.-J. Yu, H. Wang, X. Xu, Y. Liu
College of Chemistry
State Key Laboratory of Elemento-Organic Chemistry
Nankai University
Tianjin 300071, P. R. China
E-mail: yuliu@nankai.edu.cn
F.-F. Shen
Key Laboratory of Jiangxi Province for Persistent Pollutants Control and Resources Recycle
Department of Environmental and Chemical Engineering
Nanchang Hangkong University
Nanchang 330063, China
The ORCID identification number(s) for the author(s) of this article can be found under https://doi.org/10.1002/adom.202200245.

DOI: 10.1002/adom.202200245

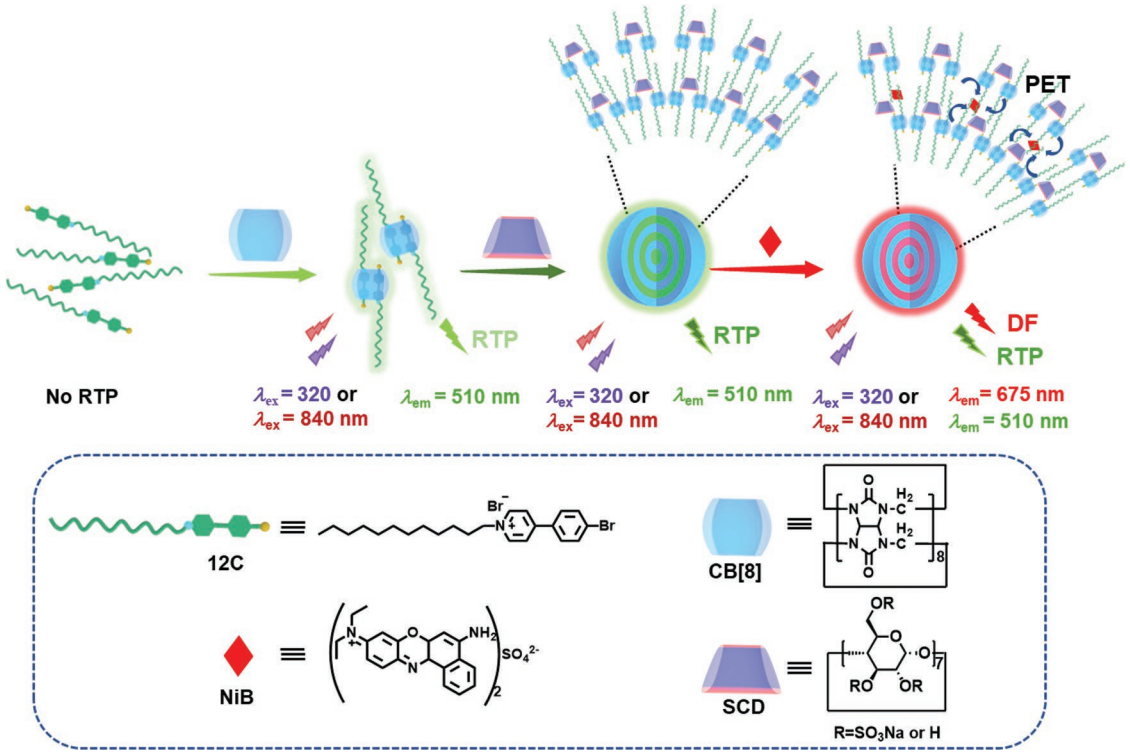

Scheme 1. Illustration of room-temperature phosphorescence (RTP) and near-infrared-delayed fluorescence (DF) (via phosphorescent energy transfer or PET) of a supramolecular assembly with a three-photon absorption property (CB[8]: cucurbit[8]uril; NiB: Nile blue; SCD: sulfonated β-cyclodextrin).

sulfonated β-cyclodextrin (SCD) led to aggregation-induced enhancement of RTP emission. Surprisingly, the supramolecular assemblies also exhibited three-photon absorption and could be excited with NIR light. Furthermore, a highly effective light-harvesting phosphorescent energy transfer (PET) system was realized when the ternary supramolecular assemblies with SCD were loaded with Nile blue (NiB). Compared with **6C**/CB[8]/SCD, **12C**/CB[8]/SCD was more effective in facilitating the NIR-delayed fluorescence emission of NiB. Ultimately, we successfully applied the supramolecular assemblies to the three-photon imaging of HeLa cells.

2. Results and Discussion

The detailed synthesis steps and characterization data of the alkyl-chain-substituted bromophenyl pyridinium salts (**6C** and **12C**) are provided in Scheme S1 and Figures S1–S6 (Supporting Information). First, we performed NMR experiments to investigate the binding mode of the guest molecules on the CB[8] host. In the ^{1}H NMR spectra (Figures S7,S8, Supporting Information), the peaks of the aromatic ring protons of **12C** and **6C** shifted upfield and broadened, while those of the alkyl chain protons of **12C** and **6C** shifted downfield and broadened, in the presence of CB[8]. This indicates that the aromatic rings are inside the CB[8] cavity and the alkyl chains are located at the CB[8] carbonyl portals. When the concentration of CB[8] reached 0.5 equiv, the chemical shifts no longer changed, demonstrating the 2:1 binding stoichiometry of the guest molecule and CB[8], which is in line with a previous report.[29]

We then explored the optical properties of the host–guest complexes. In the UV–visible spectra (**Figure 1**a), both **12C** and **6C** exhibited a maximum absorption peak at ≈307 nm in an aqueous solution. The maximum absorption peak of **12C** remained unchanged, whereas that of **6C** showed a red-shift of 8 nm upon the addition of CB[8]. In the photoluminescence spectra, a new emission peak centered at 510 nm appeared, accompanied by a decline in the original emission at ≈380 nm (Figure 1b). Unlike in the photoluminescence spectra, only the emission at 510 nm could be observed in the gated spectra (Figure 1c), revealing the long lifetime of this emission. The time-resolved decay curves and quantum yields were measured under ambient conditions. As shown in Figure 1d, the lifetimes of **12C**/CB[8] and **6C**/CB[8] at 510 nm were 0.30 and 0.39 ms, respectively, confirming that the emission at 510 nm is RTP emission. The quantum yields of **6C**/CB[8] and **12C**/CB[8] were 1.15% and 0.94%, respectively (Table S1, Supporting Information).

According to a previous report, negatively charged water-soluble cyclodextrins and calixarenes can exhibit aggregation-induced enhanced emission via noncovalent interactions.[30] To further improve RTP emission, SCD was introduced to our current system to induce aggregation. As shown in **Figure 2**a,b, the RTP emission of the **12C**/CB[8] and **6C**/CB[8] solutions markedly increased with the gradual addition of SCD. The RTP intensity of **12C**/CB[8] stopped increasing when the SCD concentration reached 8.3 μM, which was consistent with the optical transmittance results (Figure S9, Supporting Information). This demonstrates that the preferred mixing ratio of SCD and **12C**/CB[8] is 1:6. In addition, the **12C**/CB[8]/SCD aqueous solution exhibited an obvious Tyndall effect

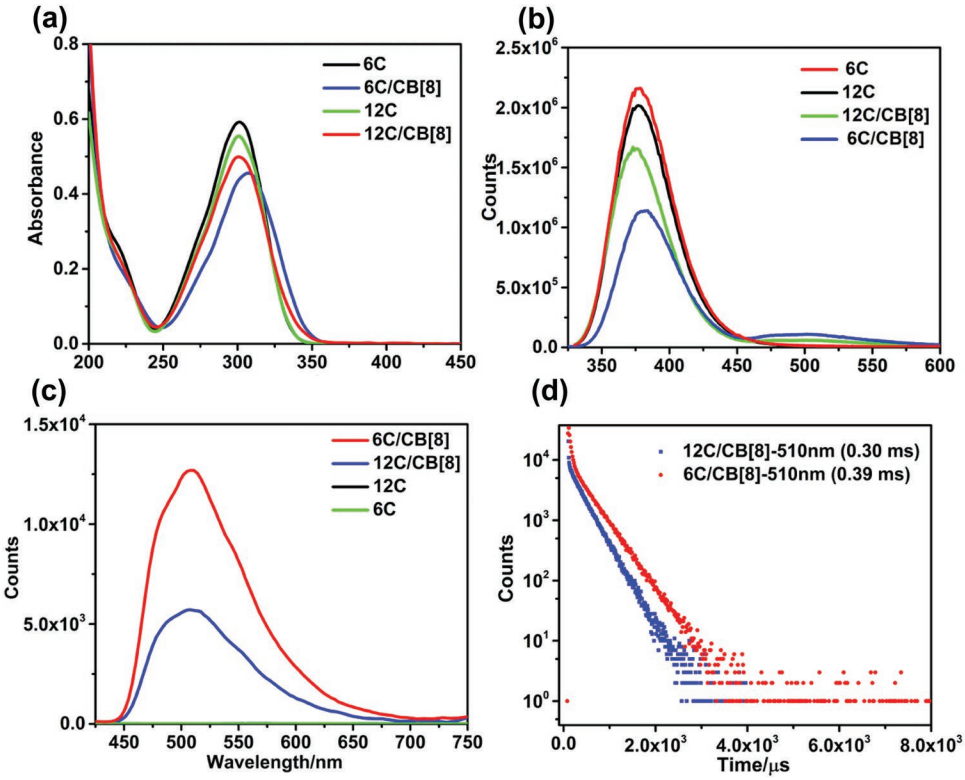

Figure 1. a) UV–visible absorption spectra of **12C**, **6C**, **12C**/CB[8], and **6C**/CB[8] in an aqueous solution ([**12C**] = [**6C**] = [CB[8]] = 0.025 mM). b) Prompt photoluminescence spectra and c) gated spectra (delay time = 0.05 ms, slit width = 5.0 nm, 5.0 nm) of **12C**, **6C**, **12C**/CB[8], and **6C**/CB[8] in an aqueous solution. d) Phosphorescence lifetime decay curves of **12C**/CB[8] and **6C**/CB[8] at 510 nm ([**12C**] = [**6C**] = [CB[8]] = 0.05 mM, λ_{ex} = 320 nm, 298 K).

(Figure S10, Supporting Information), implying the formation of supramolecular aggregates. The TEM images showed that the **12C**/CB[8]/SCD assembly formed small nanoaggregates with a diameter range of 20–80 nm, whereas **12C**/CB[8] formed large nanoaggregates with a side length range of 500–1000 nm (Figure S11, Supporting Information). As confirmed by the gated spectra, the intensity of the RTP emission of the **12C**/CB[8]/SCD assembly at 510 nm was fourfold that of **12C**/CB[8] (Figure 2c). When the same amount of SCD was added to **6C**/CB[8], the RTP intensity increased to threefold that of the original sample. The difference between the RTP intensities of **6C**/CB[8]/SCD and **12C**/CB[8]/SCD might be due to the different assembly mode and aggregation compactness caused by the difference in the alkyl chain length, which affects the microenvironment of the chromophores. Additionally, **12C**/SCD and **6C**/SCD did not exhibit RTP in the absence of CB[8], proving that CB[8] is necessary for RTP emission. Meanwhile, the maximum absorption peak of **12C**/CB[8] in the UV–visible spectrum was slightly red-shifted upon the addition of SCD, while that of **6C**/CB[8] remained basically unchanged (Figure S12, Supporting Information). Subsequently, the influence of SCD on the RTP lifetime and quantum yields was explored. The lifetimes of **12C**/CB[8]/SCD and **6C**/CB[8]/SCD at 510 nm were 0.70 and 1.26 ms, respectively (Figure 2d and Table S1, Supporting Information). The quantum yields of **12C**/CB[8]/SCD and **6C**/CB[8]/SCD were 2.74% and 3.47%, respectively (Table S1, Supporting Information). However, simply increasing the concentration of the phosphorescent group without adding SCD did not enhance the phosphorescence intensity. When the concentration was increased, the phosphorescence intensity of **6C**/CB[8] decreased, whereas that of **12C**/CB[8] remained unchanged (Figure S13, Supporting Information). The Tyndall effect of **6C**/CB[8] was more obvious, whereas that of **12C**/CB[8] was not significantly different (Figure S14, Supporting Information). The introduction of SCD into the supramolecular complexes significantly improved the RTP performance for two reasons: first, the presence of SCD restricted the movement of the phosphorescent luminophore and prevented its formation of large aggregates through electrostatic interactions, inhibited nonradiative transitions, and protected the triplet state; second, surrounding the phosphorescent group with SCD further shielded the oxygen quencher in aqueous solution. Although adding SCD resulted in aggregation-induced phosphorescence enhancement, replacing CB[8] with CB[7] did not effectively increase the phosphorescence emission (Figure S15, Supporting Information), indicating that CB[8] plays an important role in effective RTP emission.

Subsequently, considering the excellent RTP performance and hydrophobic layer of the supramolecular assembly, we expected that a long-lived NIR-delayed fluorescence emission can be realized by loading a substrate into the assembly. NiB was chosen as a suitable acceptor because its absorption spectrum partly overlaps with the RTP emission spectrum of the ternary supramolecular assembly (**Figure 3**a). When NiB was added to the **12C**/CB[8]/SCD aqueous solution, the RTP intensity at approximately 510 nm decreased, while a new emission peak

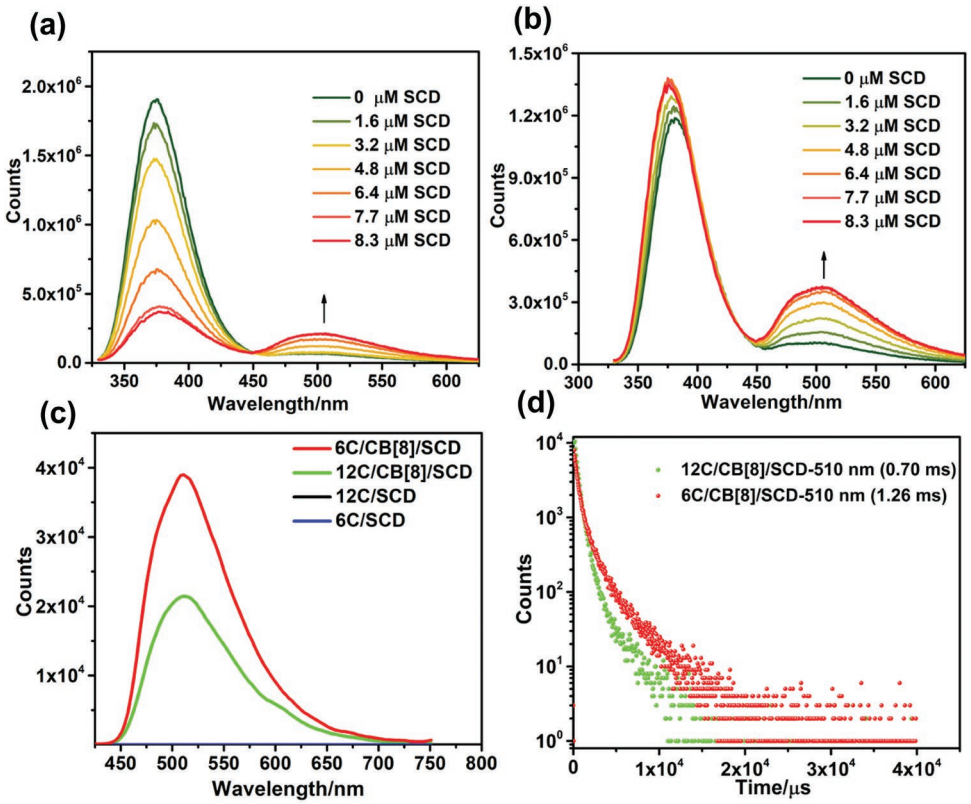

Figure 2. Prompt photoluminescence of: a) **12C**/CB[8] and b) **6C**/CB[8] in an aqueous solution with different concentrations of SCD. c) Gated spectra of **12C**/CB[8]/SCD, **6C**/CB[8]/SCD, **12C**/SCD, and **6C**/SCD in an aqueous solution. d) Phosphorescence lifetime decay curves of **6C**/CB[8]/SCD and **12C**/CB[8]/SCD at 510 nm ([**12C**] = [**6C**] = [CB[8]] = 0.05 mM, [SCD] = 0.0083 mM, λ_{ex} = 320 nm, 298 K).

centered at ≈680 nm appeared and was enhanced in the gated spectra (Figure 3b). When the donor/acceptor (D/A) molar ratio was 188:1, the emission of the acceptor reached a maximum. At a D/A molar ratio of 94:1, the lifetime at 510 nm decreased from 0.70 to 0.41 ms, and the lifetime at 680 nm was 0.13 ms (Figure S16 and Table S1, Supporting Information). Accordingly, the energy transfer efficiencies (Φ_{ET}) calculated from the lifetime and emission intensity data were 41.4% and 62.0%, respectively (Equations S1,S2 and Figure S27, Supporting Information). The antenna effect value of **12C**/CB[8]/SCD/NiB reached 152.65 (Equation S3 and Figure S28, Supporting Information). Moreover, the emission at 680 nm was consistent with the characteristic emission peak of NiB (Figure S17, Supporting Information), which clearly demonstrates the typical delayed fluorescence property of NiB emission.[18] These results indicate that light-harvesting PET occurred from the triplet state of

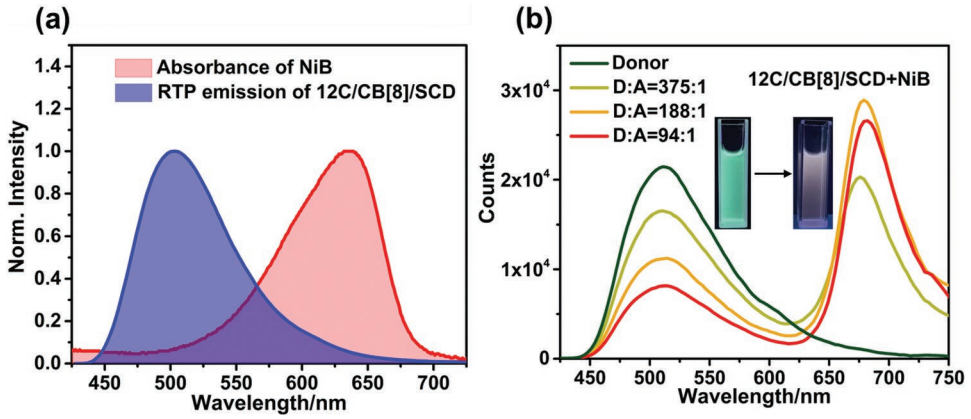

Figure 3. a) Normalized absorption spectra of Nile blue (NiB) and room-temperature phosphorescence (RTP) emission of **12C**/CB[8]/SCD. b) Gated spectra (delay time = 0.05 ms) of **12C**/CB[8]/SCD in an aqueous solution with different concentrations of NiB (inset: photographs of **12C**/CB[8]/SCD with or without NiB under UV irradiation).

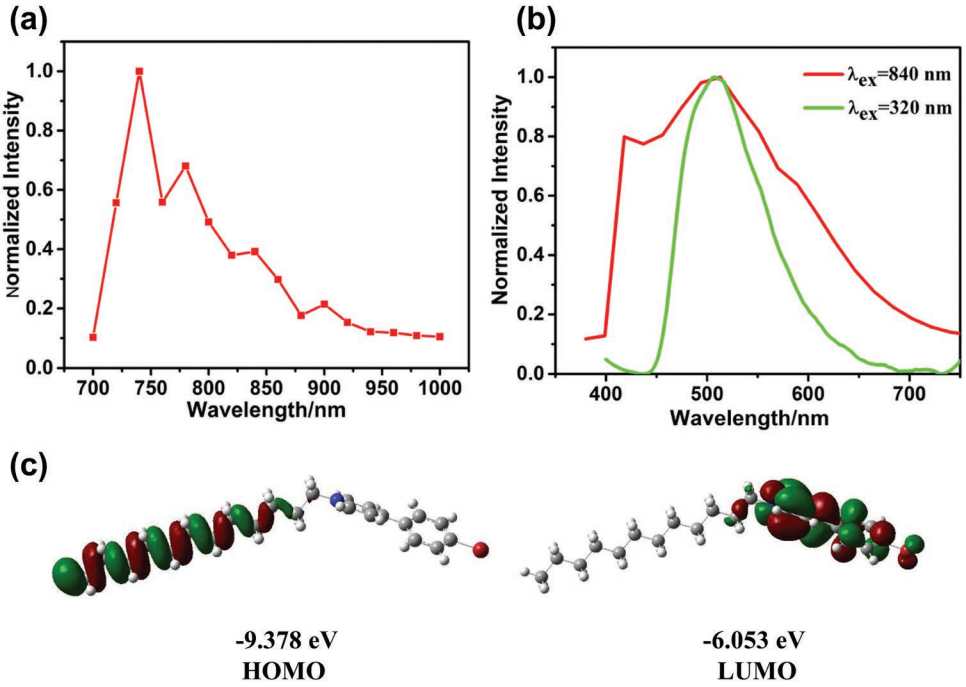

Figure 4. a) The highest occupied molecular orbital (HOMO) and lowest unoccupied molecular orbital (LUMO) orbitals of the singlet ground state of **12C** (**12C**-S_0) and the corresponding orbital energies. b) Three-photon excitation spectrum of **12C**/CB[8] in water ([**12C**] = [CB[8]] = 0.05 mM). c) Emission spectra of **12C**/CB[8] excited at 320 (green curve) and 840 nm (red curve) ([**12C**] = [CB[8]] = 0.05 mM).

12C/CB[8]/SCD to the singlet state of the NiB molecules.[18,29] As in the case of the **12C**/CB[8]/SCD system, adding a trace of NiB to **6C**/CB[8]/SCD also achieved efficient light-harvesting PET in aqueous solution (Figure S18, Supporting Information). However, the delayed fluorescence intensity at 680 nm decreased at a D/A molar ratio of 188:1, and the calculated antenna effect value of **6C**/CB[8]/SCD/NiB was 75.98. These results indicate that the longer hydrophobic layer of **12C** is more beneficial for stabilizing NIR-delayed fluorescence emission (Figures S28,S29, Supporting Information).

Multiphoton absorption (MPA) materials have been applied in many fields, such as bioimaging,[31] photodynamic therapy,[32] and photopolymerization,[33] owing to their capability of excitation by NIR light. Interestingly, the supramolecular complexes in the present work exhibited MPA property. As shown in **Figure 4**a, the excitation wavelength of **12C**/CB[8] ranged from 710 to 925 nm, as measured by femtosecond laser pulses. Under excitation at 840 or 750 nm, the maximum emission peak of the multiphoton excitation spectrum overlapped with that of the single-photon spectrum (Figures 4b and Figure S19, Supporting Information). To avoid damage to cells and interference with background fluorescence, NIR excitation light was selected for cell imaging. Therefore, we used an excitation wavelength of 840 nm in the subsequent cell experiments. We hypothesized that **12C**/CB[8] possesses a three-photon absorption property because the radiation energy for three-photon absorption at a wavelength of 840 nm falls within the UV–visible absorption range of **12C**/CB[8]. Subsequently, we explored the mechanism by which **12C**/CB[8] exhibits three-photon absorption. It is well known that a conjugated structure and internal charge transfer transitions can promote MPA.[30b,34] Next, we performed density functional theory and molecular electrostatic potential calculations to understand the inherent internal charge transfer transitions of **12C**. As shown in Figure 4c, the lowest unoccupied molecular orbital (LUMO) of the singlet ground state of **12C** (**12C**-S_0) is mainly localized at the pyridyl and bromophenyl groups, whereas the highest occupied molecular orbital (HOMO) is localized at the alkyl chain. This is consistent with the molecular electrostatic potential map (Figure S20, Supporting Information), illustrating that electron transfer from the alkyl chain to the pyridyl and bromophenyl groups may occur upon excitation of **12C**-S_0. Furthermore, the emission spectra of **12C**/CB[8]/SCD and **6C**/CB[8]/SCD excited at 840 nm also showed green RTP emission (Figures S21–S23, Supporting Information).

Subsequently, we applied the three-photon RTP and NIR-delayed fluorescence of **12C**/CB[8]/SCD/NiB and RTP emission of **12C**/CB[8]/SCD in cell-imaging experiments. HeLa cells were treated with **12C**/CB[8]/SCD/NiB and **12C**/CB[8]/SCD aggregates for 12 h. Next, we employed multiphoton microscopy to investigate the cellular distribution of the aggregates. As shown in **Figure 5**, both green and red luminescence could be observed in the cytoplasm of HeLa cells when excited by an 840-nm femtosecond pulsed laser (Figure 5a–c). Thus, the **12C**/CB[8]/SCD/NiB supramolecular nanoaggregates can be successfully applied in RTP and NIR-delayed fluorescence biological imaging by multiphoton excitation. Cytotoxicity experiments were performed on HeLa cells using Cell Counting Kit-8 assays. The viability results shown in Figure S24 (Supporting Information) demonstrated that the nanoaggregates had low cytotoxicity. Meanwhile, green emission was also observed in the three-photon microscopic image of the **12C**/CB[8]/SCD nanoparticles in Figure S25 (Supporting Information).

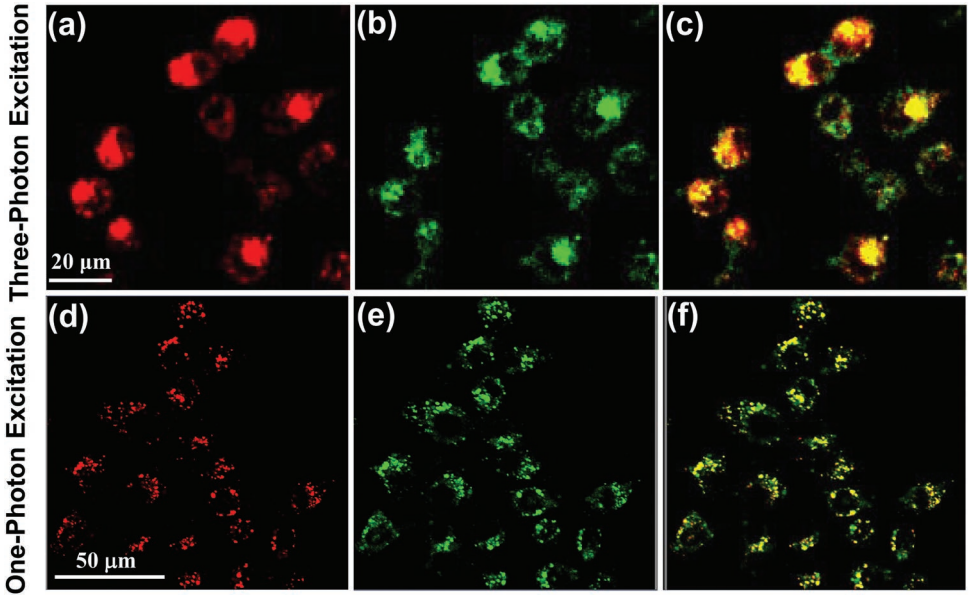

Figure 5. Three-photon microscopic images of HeLa cells incubated with **12C**/CB[8]/SCD/NiB ([**12C**] = 0.01mM) excited at 840 nm: a) red channel (650–703 nm), b) green channel (484–537 nm), and c) merged image of (a) and (b). Confocal laser scanning microscopy images of HeLa cells incubated with: d) Lyso-Tracker Red, e) **12C**/CB[8]/SCD (0.01 mM) excited at 405 nm, and f) merged image of (d) and (e).

Subsequently, confocal laser scanning microscopy was performed to investigate intracellular distribution. HeLa cells were costained with a lysosome-staining dye, Lyso-Tracker Red DND-99, and **12C**/CB[8]/SCD nanoparticles. As shown in Figure 5d–f, the merged yellow dyeing sites of green **12C**/CB[8]/SCD and red Lyso-Tracker Red, as well as the high Pearson's coefficient (0.87) of the lysosome targeting effect, demonstrated that the nanoparticles can target lysosomes in HeLa cells (Figure S26, Supporting Information).

3. Conclusion

In conclusion, we presented supramolecular nanoparticles exhibiting three-photon-excited RTP and NIR-delayed fluorescence for cancer cell imaging. In this work, the guest molecule **12C** served as a basic building block and was encapsulated in CB[8] in a head-to-tail manner to generate RTP emission upon three-photon excitation. In addition, the RTP emission strengthened after further assembly with SCD into nanoparticles, which could target the lysosomes of HeLa cells. Intriguingly, introducing NiB dye into the nanoparticles resulted in NIR-delayed fluorescence emission by highly efficient PET, which was successfully applied to the three-photon imaging of cancer cells. This purely organic supramolecular RTP system solves the problem of short excitation and emission wavelengths and provides a convenient and efficient method for application in bioimaging.

Supporting Information

Supporting Information is available from the Wiley Online Library or from the author.

Acknowledgements

The authors thank National Natural Science Foundation of China (NNSFC 22131008 and 21807038) for financial support. The cell image acquisition was supported by Biological Imaging and Analysis Laboratory, Medical and Healthy Analytical Center, Peking University, especially Jing Wu.

Conflict of Interest

The authors declare no conflict of interest.

Data Availability Statement

The data that support the findings of this study are available from the corresponding author upon reasonable request.

Keywords

NIR-delayed fluorescence, purely organic RTP materials, room-temperature phosphorescence, supramolecular assemblies, targeted imaging, three-photon absorption

Received: February 2, 2022
Revised: March 17, 2022
Published online:

[1] G. Zhang, G. M. Palmer, M. W. Dewhirst, C. L. Fraser, *Nat. Mater.* **2009**, *8*, 747.
[2] Y. Wang, H. Gao, J. Yang, M. Fang, D. Ding, B. Z. Tang, Z. Li, *Adv. Mater.* **2021**, *33*, 2007811.
[3] Q. Miao, C. Xie, X. Zhen, Y. Lyu, H. Duan, X. Liu, J. V. Jokerst, K. Pu, *Nat. Biotechnol.* **2017**, *35*, 1102.

[4] W. Qin, J. Ma, Y. Zhou, Q. Hu, Y. Zhou, G. Liang, *Chem. Eng. J.* **2021**, *419*, 129598.
[5] X.-Q. Liu, K. Zhang, J.-F. Gao, Y.-Z. Chen, C.-H. Tung, L.-Z. Wu, *Angew. Chem., Int. Ed.* **2020**, *59*, 23456.
[6] M. S. Kwon, D. Lee, S. Seo, J. Jung, J. Kim, *Angew. Chem., Int. Ed.* **2014**, *53*, 11177.
[7] Y. Su, S. Z. F. Phua, Y. Li, X. Zhou, D. Jana, G. Liu, W. Q. Lim, W. K. Ong, C. Yang, Y. Zhao, *Sci. Adv.* **2018**, *4*, eaas9732.
[8] J. Yang, M. Fang, Z. Li, *Acc. Mater. Res.* **2021**, *2*, 644.
[9] J. Zhang, S. Xu, Z. Wang, P. Xue, W. Wang, L. Zhang, Y. Shi, W. Huang, R. Chen, *Angew. Chem., Int. Ed.* **2021**, *60*, 17094.
[10] Z. An, C. Zheng, Y. Tao, R. Chen, H. Shi, T. Chen, Z. Wang, H. Li, R. Deng, X. Liu, W Huang, *Nat. Mater.* **2015**, *14*, 685.
[11] X.-K. Ma, Y. Liu, *Acc. Chem. Res.* **2021**, *54*, 3403.
[12] W. Zhao, Z. He, B. Z. Tang, *Nat. Rev. Mater.* **2020**, *5*, 869.
[13] X. Ma, J. Wang, H. Tian, *Acc. Chem. Res.* **2019**, *52*, 738.
[14] H.-J. Yu, Q. Zhou, X. Dai, F.-F. Shen, Y.-M. Zhang, X. Xu, Y. Liu, *J. Am. Chem. Soc.* **2021**, *143*, 13887.
[15] S. M. A. Fateminia, Z. Mao, S. Xu, Z. Yang, Z. Chi, B. Liu, *Angew. Chem., Int. Ed.* **2017**, *56*, 12160.
[16] a) Z.-Y. Zhang, W.-W. Xu, W.-S. Xu, J. Niu, X.-H. Sun, Y. Liu, *Angew. Chem., Int. Ed.* **2020**, *59*, 18748; b) W.-L. Zhou, Y. Chen, Q. Yu, H. Zhang, Z.-X. Liu, X.-Y. Dai, J.-J. Li, Y. Liu, *Nat. Commun.* **2020**, *11*, 4655.
[17] a) W.-W. Xu, Y. Chen, Y.-L. Lu, Y.-X. Qin, H. Zhang, X. Xu, Y. Liu, *Angew. Chem., Int. Ed.* **2022**, *61*, e202115265; b) T. Zhang, X. Ma, H. Wu, L. Zhu, Y. Zhao, H. Tian, *Angew. Chem., Int. Ed.* **2020**, *59*, 11206. c) S. Guo, W. Dai, X. Chen, Y. Lei, J. Shi, B. Tong, Z. Cai, Y. Dong, *ACS Mater. Lett.* **2021**, *3*, 379.
[18] S. Garain, B. C. Garain, M. Eswaramoorthy, S. K. Pati, S. J. George, *Angew. Chem., Int. Ed.* **2021**, *60*, 19720.
[19] J. Wang, Z. Huang, X. Ma, H. Tian, *Angew. Chem., Int. Ed.* **2020**, *59*, 9928.
[20] X.-K. Ma, W. Zhang, Z. Liu, H. Zhang, B. Zhang, Y. Liu, *Adv. Mater.* **2021**, *33*, 2007476.
[21] C. Wang, X.-K. Ma, P. Guo, C. Jiang, Y.-H. Liu, G. Liu, X. Xu, Y. Liu, *Adv. Sci.* **2021**, 2103041.
[22] X. Zhen, R. Qu, W. Chen, W. Wu, X. Jiang, *Biomater. Sci.* **2021**, *9*, 285.
[23] H. Xiang, J. Cheng, X. Ma, X. Zhou, J. J. Chruma, *Chem. Soc. Rev.* **2013**, *42*, 6128.
[24] R. Weinstain, T. Slanina, D. Kand, P. Klán, *Chem. Rev.* **2020**, *120*, 13135.
[25] S. Wang, X. Li, S. Y. Chong, X. Wang, H. Chen, C. Chen, L. G. Ng, J.-W. Wang, B. Liu, *Adv. Mater.* **2021**, *33*, 2007490.
[26] C. Jin, F. Liang, J. Wang, L. Wang, J. Liu, X. Liao, T. W. Rees, B. Yuan, H. Wang, Y. Shen, Z. Pei, L. Ji, H. Chao, *Angew. Chem., Int. Ed.* **2020**, *59*, 15987.
[27] J.-J. Li, H.-Y. Zhang, G. Liu, X. Dai, L. Chen, Y. Liu, *Adv. Optical Mater.* **2021**, *9*, 2001702.
[28] W.-C. Geng, Z. Ye, Z. Zheng, J. Gao, J.-J. Li, M. R. Shah, L. Xiao, D.-S. Guo, *Angew. Chem., Int. Ed.* **2021**, *60*, 19614.
[29] F.-F. Shen, Y. Chen, X.-Y. Dai, H.-Y. Zhang, B. Zhang, Y.-H. Liu, Y. Liu, *Chem. Sci.* **2021**, *12*, 1851.
[30] a) Z. Liu, X. Dai, Y. Sun, Y. Liu, *Aggregate* **2020**, *1*, 31; b) F.-F. Shen, Y. Chen, X. Xu, H.-J. Yu, H. Wang, Y Liu, *Small* **2021**, 2101185.
[31] a) J. H. Yu, S.-H. Kwon, Z. Petrášek, O. K. Park, S. W. Jun, K. Shin, M. Choi, Y. I. Park, K. Park, H. B. Na, N. Lee, D. W. Lee, J. H. Kim, P. Schwille, T. Hyeon, *Nat. Mater.* **2013**, *12*, 359; b) H. M. Kim, B. R. Cho, *Chem. Rev.* **2015**, *115*, 5014; c) J. Yang, Y. Zhang, X. Wu, W. Dai, D. Chen, J. Shi, B. Tong, Q. Peng, H. Xie, Z. Cai, Y. Dong, X. Zhang, *Nat. Commun.* **2021**, *12*, 4883.
[32] Y. Shen, A. J. Shuhendler, D. Ye, J.-J. Xua, H.-Y. Chen, *Chem. Soc. Rev.* **2016**, *45*, 6725.
[33] S. Wang, W. Wu, P. Manghnani, S. Xu, Y. Wang, C. C. Goh, L. G. Ng, B. Liu, *ACS Nano* **2019**, *13*, 3095.
[34] Y. Li, S. Liu, H. Ni, H. Zhang, H. Zhang, C. Chuah, C. Ma, K. S. Wong, J. W. Y. Lam, R. T. K. Kwok, J. Qian, X. Lu, B. Z. Tang, *Angew. Chem., Int. Ed.* **2020**, *59*, 12822.